Circulation: Heart Failure

ORIGINAL ARTICLE

Ca^{2+} Cycling Alteration in a Porcine Model of Right Ventricular Dysfunction

Fabrice Antigny, PhD; Rui Luo, PhD; Romain Perrier, PhD; Bastien Masson, PhD; Guillaume Fadel, MD; Grégoire Ruffenach, PhD; Anaïs Saint-Martin Willer, PhD; Ali Akamkam, MD; Julien Grynblat, MD, PhD; Xavier Jaïs, MD; Jerôme Le Pavec, MD, PhD; Simon Dang Van, MD; Dorothée Brunet, MD; Florence Lefebvre, MSc; Garance Gérard, PhD; Séverine Domenichini, PhD; Angèle Boët, MD, PhD; Julien Guihaire, MD, PhD; Ana-Maria Gomez, PhD; David Montani, MD, PhD; Jean-Pierre Benitah, PhD; Marc Humbert, MD, PhD; Olaf Mercier, MD, PhD; Jessica Sabourin, PhD

BACKGROUND: Pulmonary hypertension is a severe disease with high mortality rates due to right ventricular (RV) failure. The molecular and cellular processes involved in RV remodeling, including Ca^{2+} handling, remain elusive due to the lack of relevant animal models. In this study, we aim to understand better the pathophysiological mechanisms involved in RV failure.

METHODS: We used the chronic thromboembolic pulmonary hypertension (CTEPH) pig model, which leads to progressive RV hypertrophy and dysfunction. Cellular, molecular unbiased global transcriptional profiling and biochemical analyses were performed on RV cardiomyocytes from CTEPH and Sham-operated pigs.

RESULTS: CTEPH pigs replicated the hemodynamics and histological changes of human CTEPH features. Transcriptome analysis in Sham and CTEPH pigs revealed molecular RV remodeling close to human patients with pulmonary arterial hypertension with decompensated RV function and notably identified changes in genes involved in Ca^{2+} signaling. At the cellular level, CTEPH myocytes presented reduced L-type Ca^{2+} current in association with reduced mRNA of *CACNA1C*. Furthermore, CTEPH myocytes showed lower $[Ca^{2+}]_i$ transients, decreased sarcoplasmic reticulum Ca^{2+} content, and decreased cell shortening, related to reduced SERCA2a (Sarco/endoplasmic reticulum Ca^{2+}-ATPase isoform 2a) protein expression. Moreover, CTEPH cardiomyocytes exhibited reduced Ca^{2+} spark occurrence, which relied on smaller RyR2 (ryanodine receptor 2) clusters and T-tubule disorganization. Finally, these alterations in Ca^{2+} homeostasis were also associated with an increased store-operated Ca^{2+} entry and the de novo expression of the Ca^{2+} sensor protein STIM1L (stromal interaction molecule 1 long isoform) in CTEPH myocytes as well as in RV from human patients with pulmonary arterial hypertension.

CONCLUSIONS: Our data reveal cellular Ca^{2+} cycling remodeling that participates in the pathogenesis of RV dysfunction and may constitute therapeutic targets to limit the development of RV dysfunction.

Key Words: calcium signaling ■ excitation contraction coupling ■ humans ■ pulmonary hypertension ■ right-sided heart failure ■ swine

An intrinsic link exists between pulmonary hypertension (PH) and right ventricular (RV) dysfunction, with each one influencing the other. PH represents a group of heterogeneous diseases of the pulmonary vasculature defined by an elevation of the mean pulmonary arterial pressure >20 mm Hg at rest.[1] PH affects almost 1% of the global population and is characterized by premature morbidity and mortality. Numerous epidemiological

Correspondence to: Fabrice Antigny, PhD, Université Paris-Saclay, Inserm, UMR-S 999, Hôpital Marie Lannelongue, 133 Ave de la Résistance, F-92350 Le Plessis Robinson, France, Email fabrice.antigny@inserm.fr; or Jessica Sabourin, PhD, Université Paris-Saclay, Inserm, UMR-S 1180, Signalisation et Physiopathologie Cardiovasculaire, 17 Ave des sciences, 91400 Orsay, France, Email jessica.sabourin@universite-paris-saclay.fr
Supplemental Material is available at https://www.ahajournals.org/doi/suppl/10.1161/CIRCHEARTFAILURE.124.012293.
For Sources of Funding and Disclosures, see page 552.

Circulation: Heart Failure is available at www.ahajournals.org/journal/circheartfailure

WHAT IS NEW?

- The chronic thromboembolic pulmonary hypertension (CTEPH) model in pigs replicates the features of patients with pulmonary arterial hypertension with decompensated right ventricular (RV) function.
- At the cellular level, CTEPH myocytes present reduced L-type Ca^{2+} current in association with reduced mRNA of *CACNA1C*.
- Myocytes from CTEPH pigs have lower and slower $[Ca^{2+}]_i$ transients, decreased sarcoplasmic reticulum Ca^{2+} content associated with reduced SERCA2a (Sarco/endoplasmic reticulum Ca^{2+}-ATPase isoform 2a) protein expression, and depressed cell shortening.
- An increase in store-operated Ca^{2+} entry in association with the de novo expression of STIM1L (stromal interaction molecule 1 long isoform) is observed in RV cardiomyocytes from CTEPH myocytes and patients with pulmonary arterial hypertension.

WHAT ARE THE CLINICAL IMPLICATIONS?

- Our CTEPH pig model of RV failure replicated most of the hemodynamics, molecular, and histological changes of human RV failure features.
- Based on unbiased RNA sequencing analysis and different experiments performed at the cellular level, we found an alteration in Ca^{2+} cycling with decreased SERCA2a expression, an alteration of diastolic Ca^{2+} sparks, and increased store-operated Ca^{2+} entry that contributes to RV dysfunction in CTEPH pigs.
- Our findings could help to provide innovative targets to counteract RV dysfunction in the context of pulmonary hypertension. This model may be a cornerstone in developing better clinical approaches to slow down the progression of RV failure.

Nonstandard Abbreviations and Acronyms

CTEPH	chronic thromboembolic pulmonary hypertension
LV	left ventricular
PAH	pulmonary arterial hypertension
PH	pulmonary hypertension
RNA-seq	RNA sequencing
RV	right ventricular/right ventricle
RVF	right ventricular failure
RyR2	ryanodine receptor 2
SERCA2a	sarco/endoplasmic reticulum Ca^{2+}-ATPase isoform 2a
SOCE	store-operated Ca^{2+} entry

studies have shown that RV function is the primary determinant of the severity of PH and the most relevant predictor of the clinical outcome of patients with PH. Despite intensive research, RV failure (RVF) pathogenesis is not well elucidated, and patients with PH still die from RVF.[2] To adapt to chronic pressure overload induced by chronic pulmonary vascular diseases, the RV develops adaptive hypertrophic remodeling to maintain adequate cardiac output and ventriculo-arterial coupling. As RV contractile dysfunction, dilation, metabolic changes, RV capillary rarefaction, inflammation, and fibrosis[3,4] progress, they lead to decompensated RVF. This is characterized by increased filling pressures, diastolic and systolic dysfunction, reduced cardiac output, and ultimately causes the death of patients with PH.[5] RV dysfunction is managed by reducing fluid retention using diuretics to decrease RV preload.[6] However, these treatments do not specifically target the remodeling of the RV compartment. This may be explained by the fact that RV function is understudied compared with the left ventricular (LV) function. Defining the molecular and cellular profile of RV dysfunction is thus essential for pursuing effective therapy for RV remodeling and dysfunction. Rodent models have been commonly used to decipher the molecular mechanisms underlying the disease, but in many cases, did not match the severity seen in patients with PH.

By combining in vivo cardiac function investigations with echocardiography and Doppler, RNA sequencing (RNA-seq), biochemical analyses, and in vitro functional studies using patch-clamp and confocal Ca^{2+} imaging, we analyzed RV hemodynamics, RV histology, and intracellular Ca^{2+} handling involved in excitation-contraction coupling in chronic thromboembolic PH (CTEPH)-induced RV dysfunction in pigs. Our results demonstrate a clear ionic, morphological, and functional remodeling that participates in the pathogenesis of RV dysfunction occurring in CTEPH.

MATERIALS AND METHODS

The authors declare that all supporting data are available within the article and its online supplementary files. The antibodies and specific primers used are listed in Table S1A and S1B, respectively. More detailed methods are described in the Supplemental Material.

Patients

Pulmonary arterial hypertension (PAH) human cardiac tissues (RV and LV) for the Western blot analyses were obtained at the time of heart-lung transplantation from 4 patients with PAH: 4 patients with PAH from group 1 of World Health Organization classification (2 females and 1 male), 2 patients with PAH and Eisenmenger syndrome (2 males), 3 patients with PAH and atrial septal defect (2 males and 1 female with *SOX17* mutation), 2 patients with PAH and ventricular septal defect (1 male and 1 female), and 1 patient with CTEPH (male). Patients with PAH studied were part of the French Network on Pulmonary Hypertension, a program approved by our institutional Ethics Committee, and who had given their written informed consent (Protocol N8CO-08-003, ID RCB: 2008-A00485-50, approved June 18, 2008). All human tissue was obtained with written and

informed consent from transplant recipients or families of organ donors in accordance with the Declaration of Helsinki.

Animal Studies and Ethics

All experiments were performed according to the European Community guiding principles in the care and use of animals (2010/63/UE, September 22, 2010), the local Ethics committee (CEEA26 CAP-Sud) guidelines, and the French decree no2013-118, February 1, 2013, on the protection of animals used for scientific purposes (JORF no0032, February 7, 2013, p 2199, text no 24). Animal experiments were approved by the French Ministry of Agriculture (agreements No14-027 and No2016-125-7914).

We induced a CTEPH model as previously described[7–9] in 7 large white male piglets aged 3 weeks at the initiation of the protocol. Premedication was achieved using intramuscular injection of an equimolar mixture of tiletamine and zolazepam (10 mg/kg) 30 minutes before the surgical procedure. General anesthesia was induced with an intravenous bolus of propofol (2 mg/kg) combined with administration of atracurium (2 mg/kg). Orotracheal intubation was established using a 7.5 mm probe to allow for mechanical ventilation (tidal volume of 6 mL/kg, positive end-expiratory pressure set at 5 cm H_2O, and 40% of inspired oxygen fraction). General anesthesia was maintained using inhaled isoflurane (expiratory fraction from 1% to 4%) and buprenorphine (0.01 mg/kg boluses). The respiratory rate was adjusted to target an end-tidal CO_2 level between 35 and 40 mm Hg and oxygen saturation above 95%. Euthanasia will be performed by an anesthetic overdose of pentobarbital sodium (150 mg/kg IV).

To achieve CTEPH modeling, we performed ligation of the left pulmonary artery and iterative embolization of the right lower lobe once a week for 6 weeks, utilizing a biological glue (enbucrilate, Histoacryl; B.Braun, Melsungen, Germany) mixed with an equivalent volume of lipiodol. We injected 1 to 4 mL of enbucrilate–lipiodol solution each week into the right lower pulmonary artery through a venous catheter inserted percutaneously through the jugular vein under fluoroscopic control.

Statistical Analysis

Analyses were performed using GraphPad Prism software (GraphPad, version 9.0 for Windows) and R statistical computing software. After checking with the Shapiro-Wilk, Kolmogorov-Smirnov, D'Agostino and Pearson, and Anderson-Darling normality tests whether the sample data followed a normal distribution, differences between the 2 groups were assessed using an unpaired *t* test. When conditions for parametric tests were not met, we used either a Mann-Whitney *U* test or the data were submitted to an Aligned Rank Transform procedure in the ARTool R package, which allowed a nonparametric factorial ANOVA considering the multiple observations per animal (Nested analysis). Correlations between variables were assessed using the 2-tailed correlation test and Pearson test. For all experiments, a *P* value of <0.05 was considered statistically significant (Table S2).

RESULTS

Hemodynamic and Molecular Remodeling of Right Ventricles From CTEPH Pigs

CTEPH pigs presented no significant differences in the weights and body surfaces compared with age-matched Sham-operated pigs (Figure S1A and S1B). The mean pulmonary arterial pressure (mean PAP; Figure 1A) measured by right heart catheterization was increased, as well as systolic and diastolic PAP (Figure S1C and S1D). This was associated with elevated total pulmonary resistance (Figure 1B). As illustrated in the short parasternal axis and the apical 4-chamber views from echocardiography (Figure 1C and 1E), CTEPH pigs developed leftward deviation of the interventricular septum and, for some of them, pericardial effusion. We found an increase in end-diastolic and end-systolic RV diameters (Figure 1F and 1G) and RV free wall thickness enlargement (Figure 1H), indicating RV hypertrophy and dilation in CTEPH pigs. We also observed a decrease in RV fractional area change (Figure 1I). Moreover, the tricuspid annular plane systolic excursion was decreased in CTEPH pigs (Figure 1J), as well as the tricuspid annular plane systolic excursion/systolic PAP ratio (Figure 1K), demonstrating an RV dysfunction associated with decreased ventricular-arterial coupling.

RV histological analyses revealed that there was an increase in RV cardiomyocyte size in the CTEPH condition (Figure 1L). By patch-clamp, we confirmed RV myocyte hypertrophy by observing enhanced cell membrane capacitance in isolated RV cardiomyocytes from CTEPH pigs (Figure 1M). These results are consistent with macroscopic RV enlargement measured by echocardiography. We also found increased RV fibrosis deposition in CTEPH pigs (Figure 1N). These in vivo changes in the pulmonary circulation, cardiac function, and RV histology represented the features of patients suffering from CTEPH.

Analysis of RV Transcriptome From CTEPH Pigs With RV Dysfunction and Comparative Transcriptome Profile of Pig and Human With RV Dysfunction

We conducted RNA-seq to profile the transcriptome of RV tissues from 5 Sham and 5 CTEPH pigs. Through the RNA-seq experiments, we detected 15 639 different genes. The raw and processed data were accessible under the accession number GSE284258. Principal component analysis showed clear, distinct patterns of the gene expression profiles for Sham and CTEPH animals (Figure 2A). RNA-seq analysis revealed 1586 differentially expressed genes between Sham and CTEPH conditions ($P<0.05$ and absolute fold change >1.5). Among these genes, 775 were downregulated, and 811 were upregulated in RV tissues from CTEPH pigs compared with Sham pigs (Figure 2B; Table S3). We found that the upregulated genes were predominantly involved in lipid metabolism, morphogenesis, development, signaling pathway, cell differentiation, and transport (Figure 2C). RNA-seq analysis also identified the

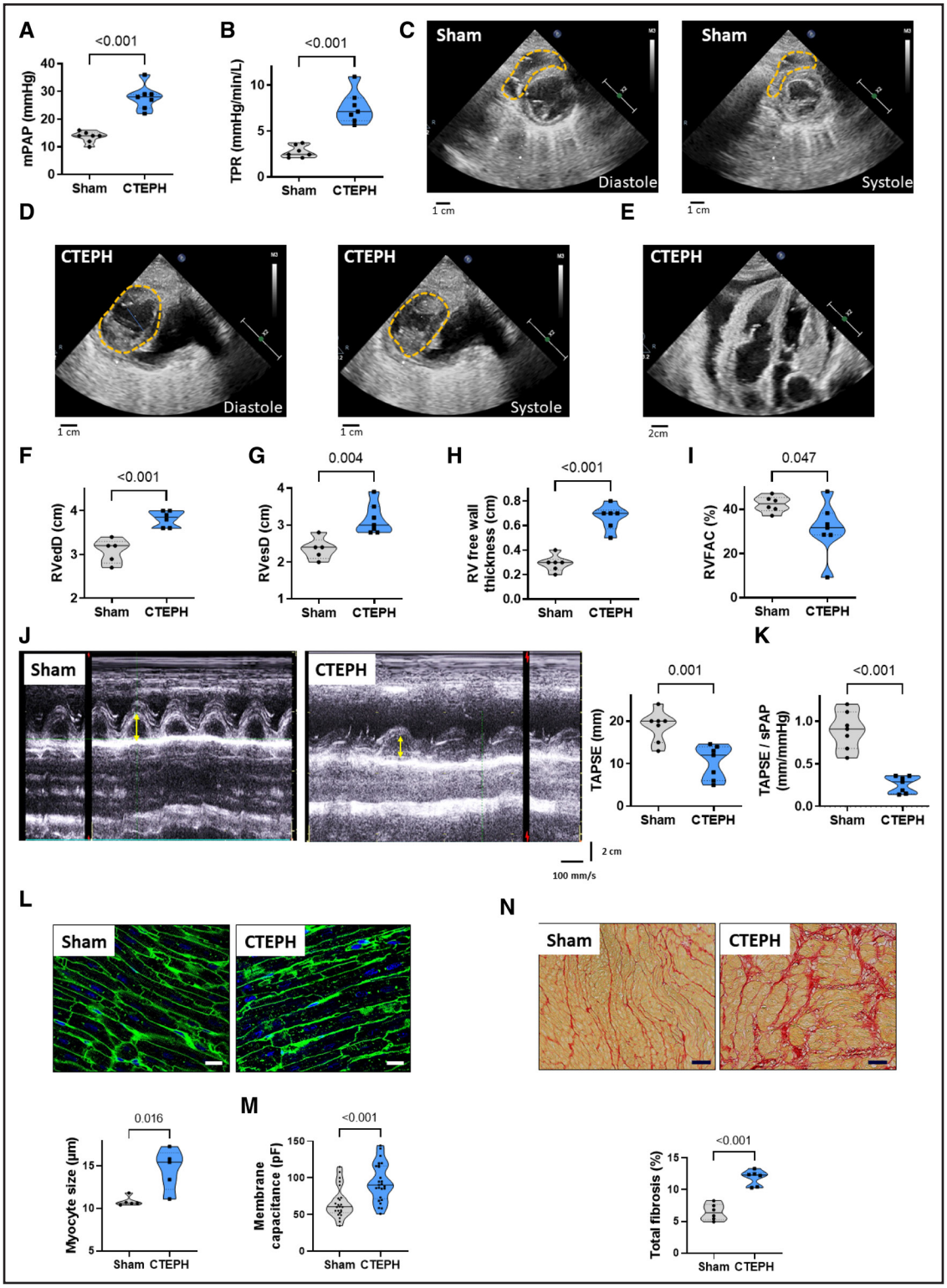

Figure 1. Characterization of right ventricular (RV) dysfunction and remodeling in chronic thromboembolic pulmonary hypertension (CTEPH) pigs.

Quantification of mean pulmonary arterial pressure (mPAP, **A**), and total pulmonary resistance (TPR, **B**). Representative echocardiographic images from Sham (**C**) and CTEPH (**D**) pigs for diastolic and systolic measurement of RV diameters in the parasternal short-axis view, showing RV enlargement and deformation in CTEPH pigs (dotted orange lines). **E**, Representative echocardiographic images from CTEPH pigs in a 4-chamber view showing intraventricular septum deviation and pericardial effusion in CTEPH pigs. **F** through **I**, Quantification of RV end-diastolic (RVedD, **F**) and systolic diameters (RVesD, **G**), RV free wall thickness (**H**), and RV fractional area change (RVFAC, **I**). **J**, Representative echocardiographic images for the measurement of the tricuspid annular plane systolic excursion (TAPSE) in M-mode view of Sham and CTEPH pigs. **Right**, Quantification of the TAPSE. The yellow arrows correspond to the distance of the tricuspid annular longitudinal (*Continued*)

downregulation of several pathways, including ions and contraction, apoptotic signaling, immune cell recruitment, enzymatic activity, mitosis, membrane organization, and mitochondrial function (Figure 2C). In more detail, we found changes in 157 genes associated with pro-hypertrophic, pro-fibrosis, or proinflammatory remodeling (Table S3). Among the most dysregulated genes, there was a substantial increase in expression of *NPPB* (Natriuretic Peptide B), *MYO7B* (Myosin VIIB), *ACTA1* (Actin α1), *TNNT1* (Troponin T1), *COL8A1* (Collagen Type VIII α1 Chain), and *COL4A5* (Collagen Type IV α5 Chain). Conversely, we observed a decrease in the expression of *LEPR* (Leptin Receptor) and *EDF1* (Endothelial Differentiation Related Factor 1). Furthermore, the CTEPH pigs were characterized by changes in various PAH predisposing genes including decrease in *SOX17* (SRY-Box Transcription Factor 17), *AQP1* (Aquaporin 1), *ACVRL1* (Activin A Receptor-Like Kinase 1), and increase in *TBX4* (T-Box Transcription Factor 4), *ATP13A3* (ATPase 13A3), and *TGFB2* (Transforming Growth Factor-β 2; Table S4). The RNA-seq analysis also showed an increase in the expression of *STMP1* (Short Transmembrane Mitochondrial Protein 1), *ACO17* (Aconitase 1), *MTFR2* (Mitochondrial Fission Regulator 2), and a reduced expression of *TOMM7* (Translocase of Outer Mitochondrial Membrane 7), *NOX5* (NADPH Oxidase 5), *MSS51* (MSS51 Mitochondrial Translational Activator), and *LDHD* (Lactate Dehydrogenase D; Table S5). This corroborated the compromised structural mitochondria integrity as evidenced by abnormalities in cristae, swelling, lipidic vacuole, structure impairments, and membrane alteration, assessed by electronic microscopy (Figure S2). In addition, changes in gene expression of 112 kinases were noticed, including reduced expression of *ROS1* (Receptor Tyrosine Kinase C-Ros Oncogene 1) and increased expression of *HASPIN* (Histone H3 Associated Protein Kinase), *RCAN1* (Regulator of Calcineurin 1), *NEK2* (NIMA Related Kinase 2) and *CAMKK1* (Ca^{2+}/Calmodulin-Dependent Protein Kinase 1) in RV tissues from CTEPH pigs compared with Sham pigs (Table S6). Finally, phosphodiesterases, known contributors to cardiac remodeling, exhibited variations. Specifically, there was increased phosphodiesterase12, phosphodiesterase8A, and phosphodiesterase6D expression and decreased phosphodiesterase4C, phosphodiesterase4A, and phosphodiesterase2A in RV tissue from CTEPH pigs (Table S7).

We also compared transcriptomic data from the CTEPH pig model and patients with compensated or decompensated RV function secondary to PAH. We revealed the proximity between molecular signatures in CTEPH pigs and decompensated Humans with 517 genes commonly dysregulated (Figure 3A).

As illustrated in Figure 3B, pathway analysis found that several dysregulated genes in RV tissues from CTEPH pigs were involved in the regulation of cellular Ca^{2+} homeostasis, cardiac AP, electrical cardiac conduction, and cardiac muscle cell communication. We thus explored the Ca^{2+} homeostasis involved in excitation-contraction coupling in RV myocytes from CTEPH pigs.

Decreased L-Type Ca^{2+} Current in RV Cardiomyocytes From CTEPH Pigs

Using the whole-cell patch-clamp, we found that the L-type Ca^{2+} current (I_{CaL}) was decreased in RV myocytes from CTEPH pigs compared with Sham (Figure 4A and 4B), as assessed by the reduced maximum conductance (Figure 4C) without changes in voltage- and time-dependent kinetics (Figure S3A through S3D). In line with decreased I_{CaL}, the *CACNA1C* gene was reduced in the RNA-seq data in association with the auxiliary subunits *CACNB2* and *CACNB4* (Figure 4D). The decrease in *CACNA1C* expression was confirmed by RT-qPCR experiments (Figure 4E). However, we found no statistical changes in the action potential (AP) amplitude (Sham: mean±SE was 128±3 mV, n=11 cells; CTEPH: mean±SE was 123±2 mV, n=17 cells) and AP duration (APD) evaluated at 20%, 50%, and 90% repolarization (Figure S4A and S4B) in RV myocytes from CTEPH pigs in comparison with Sham. Using the voltage-ramp protocol, we observed no statistical differences in inward rectifier potassium current (I_{K1}) between RV myocytes from CTEPH and Sham pigs (Figure S4C).

Alteration of Ca^{2+} Cycling in RV Cardiomyocytes From CTEPH Pigs

Because I_{CaL} was decreased, we analyzed electrically evoked $[Ca^{2+}]_i$ transients and cell shortening in RV cardiomyocytes by confocal microscopy (Figure 5A). $[Ca^{2+}]_i$ transients amplitude was significantly lower (Figure 5B), and the time to peak was longer in CTEPH myocytes

Figure 1 Continued. excursion between end-diastole and peak systole (mm). **K**, Quantification of TAPSE/systolic PAP ratio (n=7 pigs). **L**, Analysis of the level of RV cardiomyocyte hypertrophy in Sham and CTEPH pigs. **Top**, Representative confocal images of RV sections from Sham and CTEPH pigs stained with FITC-conjugated wheat germ agglutinin (WGA, 50 mg/mL). **Bottom**, Quantification of cardiomyocyte size (10 images per animal from 5 pigs; scale bar=20 μm). **M**, Membrane capacitance of RV cardiomyocytes from Sham and CTEPH pigs (n=24 cells for Sham and 25 cells for CTEPH from 5 pigs). **N**, **Top**, Representative confocal images of interstitial fibrosis identified with Sirius red staining in RV sections from Sham and CTEPH pigs. **Bottom**, Quantification of the percentage of fibrosis in RV sections from Sham and CTEPH pigs (n=10 images per pig from 6 pigs). Scale bar=50 μm. All the results are presented as violin plots showing all animals with the minimum to maximum, with the median (line), and with first and third quartiles (dotted lines). Specific procedure analysis and output for each figure panel are given in Table S2 and no outliers were eliminated.

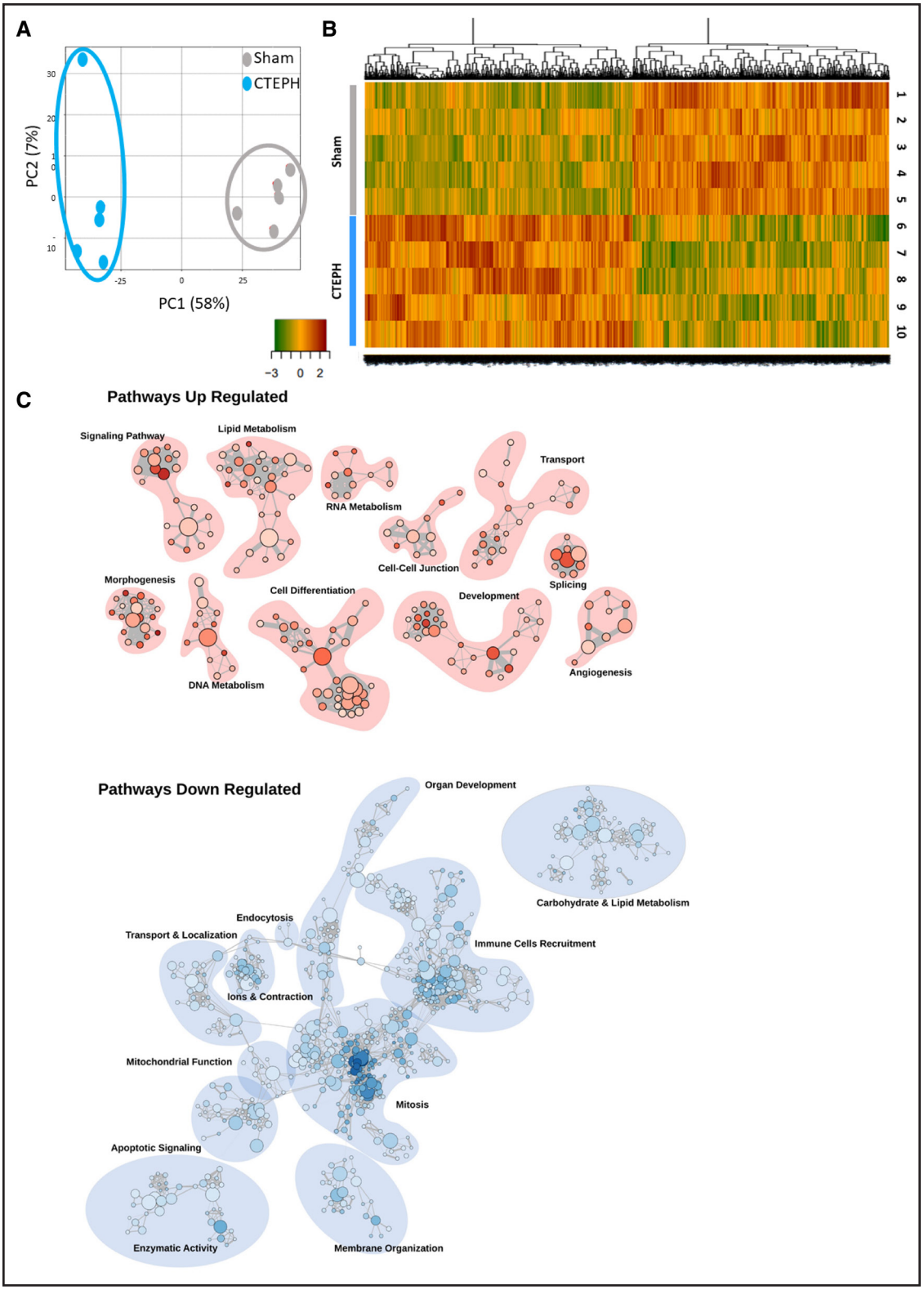

Figure 2. Characterization of right ventricular (RV) molecular remodeling in chronic thromboembolic pulmonary hypertension (CTEPH) pigs in comparison with Sham pigs.

A, Principal component analysis (PCA) was performed on the relative gene expression level between RV tissues from Sham and CTEPH pigs obtained by spectral counting (Sham [gray] or CTEPH [blue]; n=5 pigs). **B**, Heatmap Representation for RNA sequencing results in RV tissues from Sham and CTEPH pigs. **C**, Visualization of biological process gene ontology gene set enrichment analysis on the pig RNA sequencing (RNA-seq) data using the Cytoscape software. This visualization highlights the clusters of pathways upregulated (red) or downregulated (blue) involved in specific cellular functions such as ions and contraction or signalization.

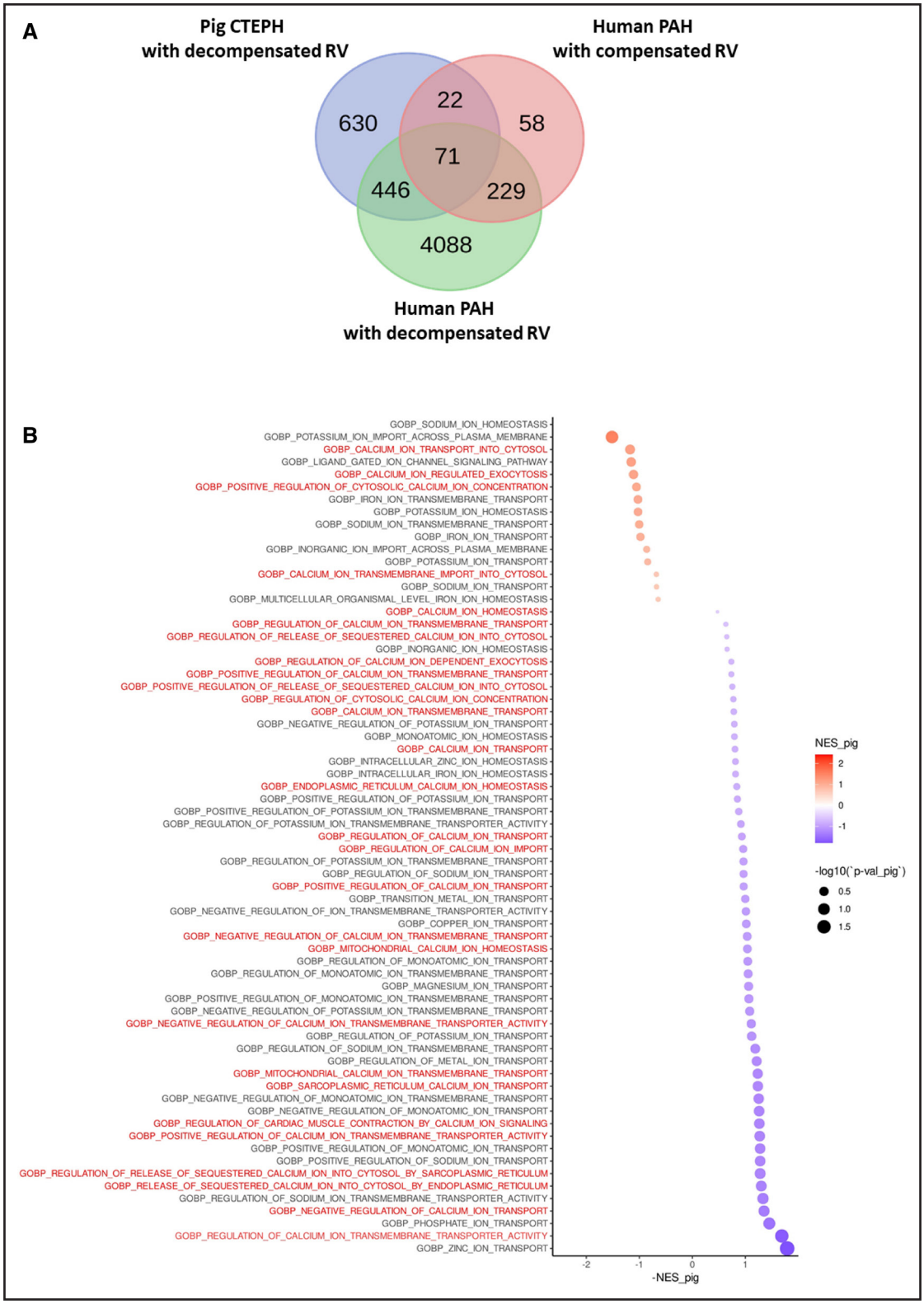

Figure 3. Comparison of right ventricular (RV) transcriptome from chronic thromboembolic pulmonary hypertension (CTEPH) pigs and human patients with pulmonary arterial hypertension (PAH).
A, Venn diagram showing the number of genes similarly dysregulated in pig CTEPH RV and human RV in a compensated or decompensated state. **B**, Pathways overview identified with reactome pathway analysis of the differentially expressed genes between RV tissues from Sham and CTEPH pigs. The red titles correspond to the Ca^{2+}-dependent pathways that were dysregulated in CTEPH pigs.

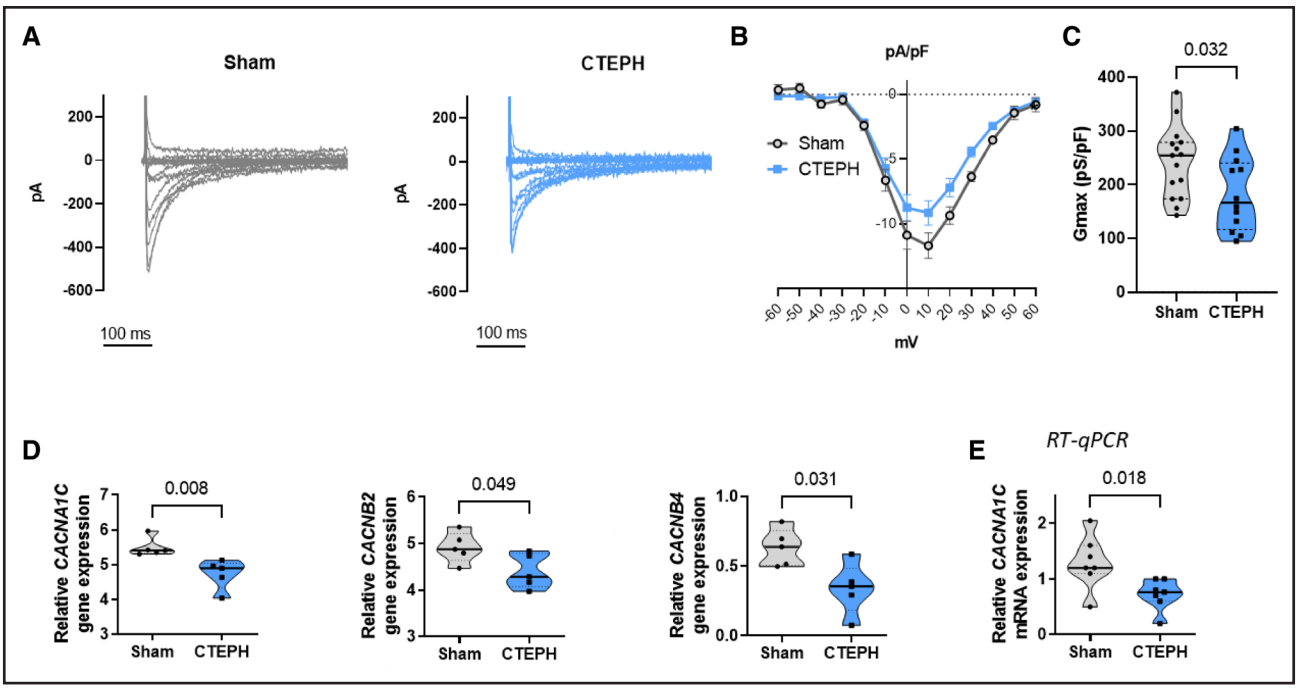

Figure 4. Reduced I_{CaL} in right ventricular (RV) cardiomyocytes from chronic thromboembolic pulmonary hypertension (CTEPH) pigs.

A, Representative I_{CaL} current traces in RV cardiomyocytes from Sham (gray traces) and CTEPH pigs (blue traces). **B**, Averaged current-voltage (I_{CaL}–V) relationships of I_{CaL} densities in freshly isolated RV cardiomyocytes from Sham and CTEPH pigs (n=15 cells for 4 Sham pigs and 12 cells for 4 CTEPH pigs). **C**, Quantification of maximum conductance (G_{max}) of I_{CaL} in freshly isolated RV cardiomyocytes from Sham and CTEPH pigs (n=15 cells for Sham and 12 cells for CTEPH from 3 pigs). **D**, Comparison of the relative gene expression of *CACNA1C* (Calcium Voltage-Gated Channel Subunit α1 C), *CACNB2* (Calcium Voltage-Gated Channel Auxiliary Subunit β 2), and *CACNB4* (Calcium Voltage-Gated Channel Auxiliary Subunit β 4) in RV from Sham and CTEPH pigs, obtained by RNA sequencing (n=5 pigs). **E**, Relative mRNA expression of *CACNA1C* obtained by RT-qPCR (n=7 pigs). All the results are presented as violin plots showing all investigated cells or animals or with the minimum to maximum, with the median (line), and with first and third quartiles (dotted lines). Specific procedure analysis and output for each figure panel are given in Table S2, and no outliers were eliminated.

compared with Sham myocytes (Figure 5C). The decay time was not significantly different but tended to be slower (Figure 5D). The decreased $[Ca^{2+}]_i$ transients amplitude was associated with a decrease in cell shortening in RV myocytes from CTEPH pigs (Figure 5E). This is consistent with the systolic dysfunction found by echocardiography as assessed by the correlation between the cell shortening and the RV fractional area change, tricuspid annular plane systolic excursion/systolic PAP, or cardiac output (Figure 5F and 5H). We saw that the Ca^{2+} release was nonsynchronous in the RV myocytes from CTEPH pigs, showing spatial heterogeneity, with a delayed increase of $[Ca^{2+}]_i$ in several areas (Figure 5I). RV myocytes from CTEPH pigs exhibited more heterogeneities with a higher variance of the rising times of the $[Ca^{2+}]_i$ transients than Sham cells (Figure 5J).

Reduced SR Ca^{2+} Content in RV Cardiomyocytes From CTEPH Pigs

As SR Ca^{2+} content is crucial to govern $[Ca^{2+}]_i$ transients amplitude, we estimated the total SR Ca^{2+} load by caffeine application in paced cells, as shown in Figure 6A. Caffeine-mediated $[Ca^{2+}]_i$ transients amplitude was smaller in CTEPH myocytes than in Sham cells (Figure 6B). The caffeine-evoked $[Ca^{2+}]_i$ transients decay time was not significantly changed in RV myocytes from Sham and CTEPH pigs (Figure 6C), suggesting preserved Na^+/Ca^{2+} exchanger activity. The weaker $[Ca^{2+}]_i$ transients amplitude could thus be due to the diminished SR Ca^{2+} load. The fractional release was also decreased in CTEPH myocytes compared with Sham myocytes (Figure 6D), suggesting that besides the decrease in SR Ca^{2+}, an additional defect accounts for the depressed $[Ca^{2+}]_i$ transients.

Because the $[Ca^{2+}]_i$ transients amplitude and decay kinetics depend on Ca^{2+} reuptake to the SR by SERCA2a (Sarco/endoplasmic reticulum Ca^{2+}-ATPase isoform 2a), which is modulated by phospholamban, we assessed their protein expression levels by Western blot. In RV tissue, the protein expression level of SERCA2a was decreased in the CTEPH group (Figure 6E), while the total phospholamban level was maintained (Figure 6F). The phosphorylation status of phospholamban by protein kinase A at the serine 16 site or by Ca^{2+}/calmodulin-dependent kinase II (CaMKII) at the threonine 17 site was preserved (Figure 6G).

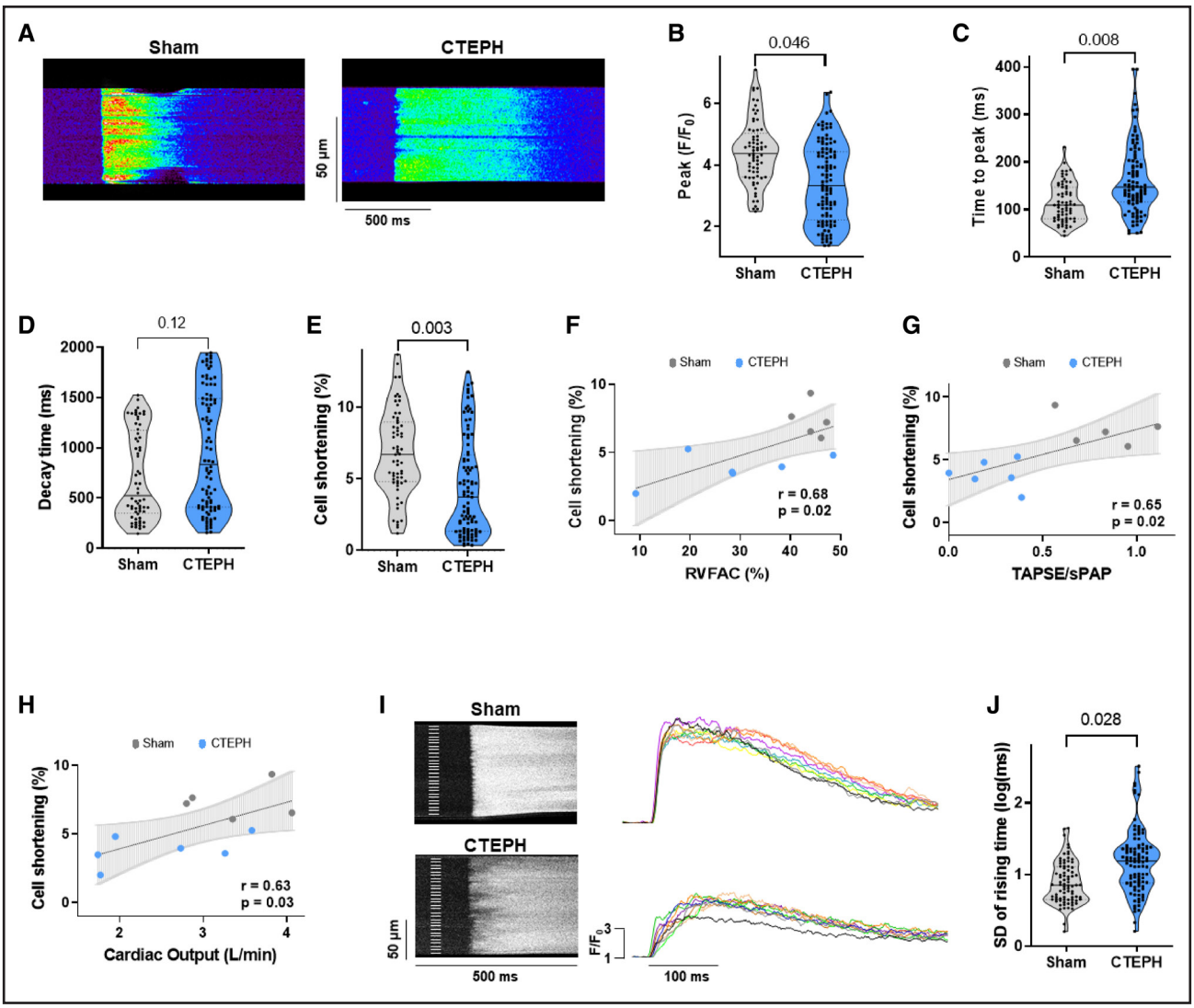

Figure 5. Stimulated $[Ca^{2+}]_i$ transients in right ventricular (RV) cardiomyocytes from Sham and chronic thromboembolic pulmonary hypertension (CTEPH) pigs.

A, Representative line-scan of $[Ca^{2+}]_i$ transients in RV cardiomyocytes field-stimulated at 0.5 Hz and loaded with Fluo-4/AM from Sham and CTEPH pigs. Average of $[Ca^{2+}]_i$ transients amplitude (peak F/F_0, **B**), of $[Ca^{2+}]_i$ transients time to peak (ms, **C**) and decay time constant (ms, **D**), and of % of the cell shortening (**E**) obtained in RV myocytes field-stimulated at 0.5 Hz from Sham and CTEPH pigs (n=5–6 pigs, n=69–108 investigated cells). **F**, Correlation between percentage of cell shortening and RVFAC of corresponding pigs. **G**, Correlation between percentage of cell shortening and the tricuspid annular plane systolic excursion (TAPSE)/ systolic PAP ratio of corresponding pigs. **H**, Correlation between percentage of cell shortening and cardiac output of corresponding pigs. **I**, **Left**, Representative line-scan images of inhomogeneous $[Ca^{2+}]_i$ transients at steady-state stimulation in RV myocytes from Sham and CTEPH pigs with the corresponding superimposed traces (**right**) taken at every 5 µm subregion noted on the left of line-scan images. **J**, Ca^{2+} release heterogeneity was quantified by the SD of the rising time of the $[Ca^{2+}]_i$ transients for Sham and CTEPH cardiomyocytes (n=5–6 pigs, n=81–99 investigated cells). All the results are presented as violin plots showing all investigated cells with the minimum to maximum, with the median (line), and with first and third quartiles (dotted lines). Specific procedure analysis and output for each figure panel are given in Table S2, and no outliers were eliminated.

Alteration of RyR2 Clusters Function and Nanostructure in RV Cardiomyocytes From CTEPH Pigs

We then evaluated diastolic Ca^{2+} release events as Ca^{2+} sparks that reflected in situ RyR2 (ryanodine receptor 2) function. Figure 7A shows examples of line scan confocal images of Ca^{2+} sparks in RV cells from Sham and CTEPH pigs. We found a decrease in Ca^{2+} sparks frequency in CTEPH myocytes in comparison with Sham myocytes (Figure 7B), which may be the result of the lower SR Ca^{2+} load. The amplitude, the full duration, and the full width at half-maximum of the Ca^{2+} sparks were not statistically different between Sham and CTEPH myocytes (Figure 7C and 7E). The Ca^{2+} release per Ca^{2+} spark, called Ca^{2+} spark mass, and the Ca^{2+} spark-mediated Ca^{2+} leak were also unchanged (Figure 7F and 7G).

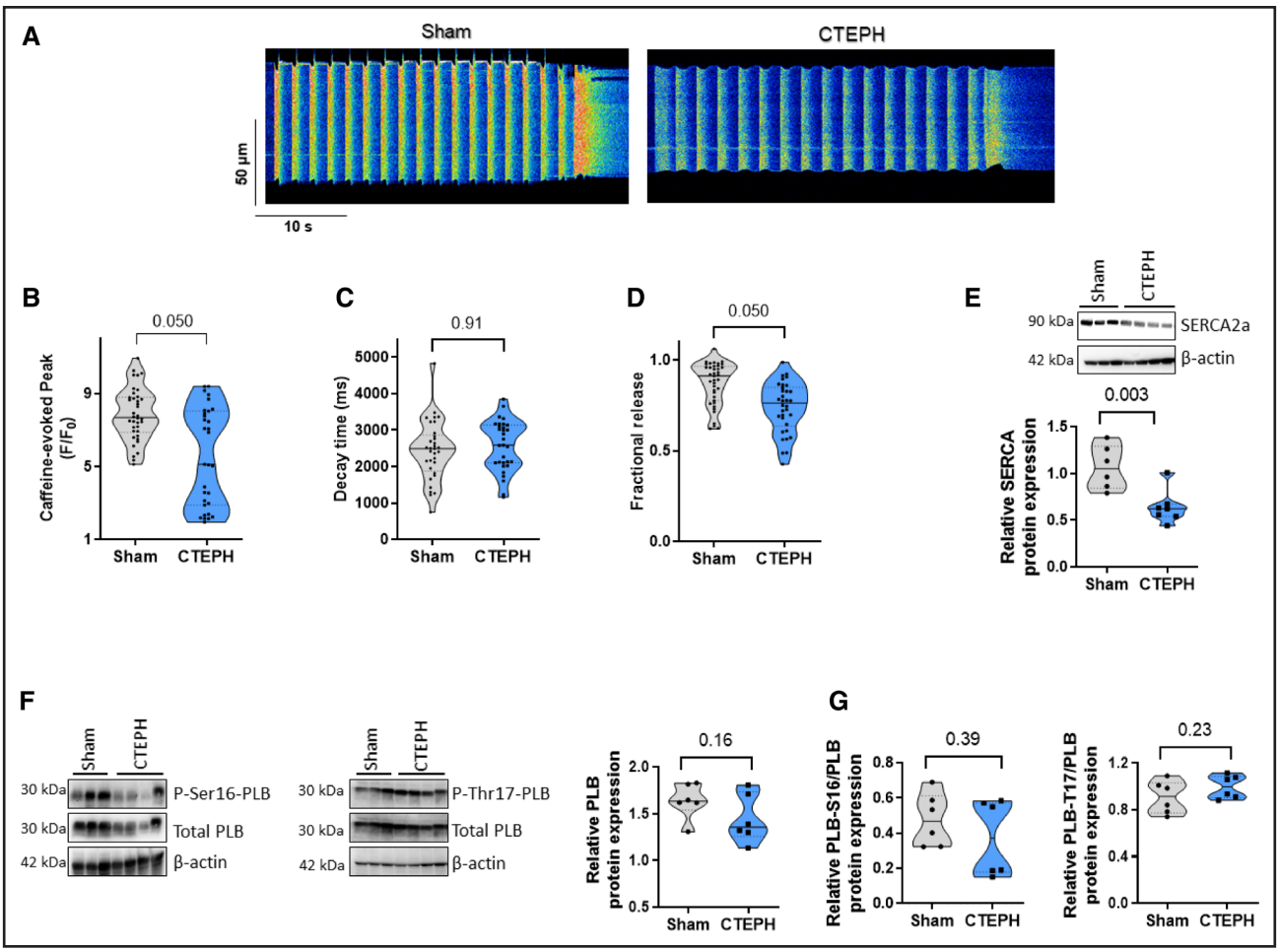

Figure 6. Sarcoplasmic reticulum (SR) Ca^{2+} content in right ventricular (RV) cardiomyocytes from Sham and chronic thromboembolic pulmonary hypertension (CTEPH) pigs.

A, Representative line-scan of caffeine-evoked $[Ca^{2+}]_i$ transients in RV cardiomyocytes field-stimulated at 0.5 Hz and loaded with Fluo-4/AM from Sham and CTEPH pigs. Average of caffeine-evoked SR Ca^{2+} load amplitude (peak F/F_0, **B**), caffeine-evoked SR Ca^{2+} load decay time constant (ms, **C**), and fractional release (**D**) recorded in RV cardiomyocytes from Sham and CTEPH pigs (n=4 pigs, n=31–39 investigated cells). **E**, Representative Western blot and quantification of SERCA2a (sarco/endoplasmic reticulum Ca^{2+}-ATPase isoform 2a) protein expression in RV tissues from Sham and CTEPH pigs. β-Actin was used as the loading control (n=6–7 pigs). **F** and **G**, Representative Western blots and quantification of total phospholamban, P-Ser16-phospholamban, and P-Thr17-phospholamban normalized by the total phospholamban expression in RV tissues from Sham and CTEPH pigs (n=6 pigs). All the results are presented as violin plots showing all investigated cells or tissues with the minimum to maximum, with the median (line), and with first and third quartiles (dotted lines). Specific procedure analysis and output for each figure panel are given in Table S2, and no outliers were eliminated.

To study whether RyR2 cluster size and distribution were affected in CTEPH conditions, we used stimulated emission-depletion super-resolution confocal microscopy in Sham and CTEPH cardiomyocytes stained with RyR2 antibody. Figure 7H showed deconvoluted images of RyR2 Ca^{2+} release units on Sham and CTEPH cells. We observed a difference in cluster size distribution, with smaller clusters being more frequent in the CTEPH condition (Figure 7I). Furthermore, Ca^{2+} release units distribution in CTEPH cells displayed greater dispersion along the Z line, with a higher relative frequency of clusters far from the line and less alignment (Figure 7J). The decreased Ca^{2+} release units size could be attributed to a decrease in RyR2 expression. However, the total RyR2 protein expression and the phosphorylation status of RyR2 at the PKA-mediated site (Ser2808) or the CaMKII-mediated site (Ser2814) were preserved in RV from CTEPH tissue (Figure 7K and 7L). As the regular alignments reflect the dyads, where junctional SR aligns with the T-tubules, in another set of experiments, we used a membrane fluorescence marker to image the T-tubules network. As shown in Figure 7M, we found a loss in the T-tubule network integrity in CTEPH cells. In the RNA-seq database, we found no significant changes in the T-tubule/SR dyadic actors such as junctophilin and telethonin genes in the RV from CTEPH pigs compared with the Sham group (Figure S5).

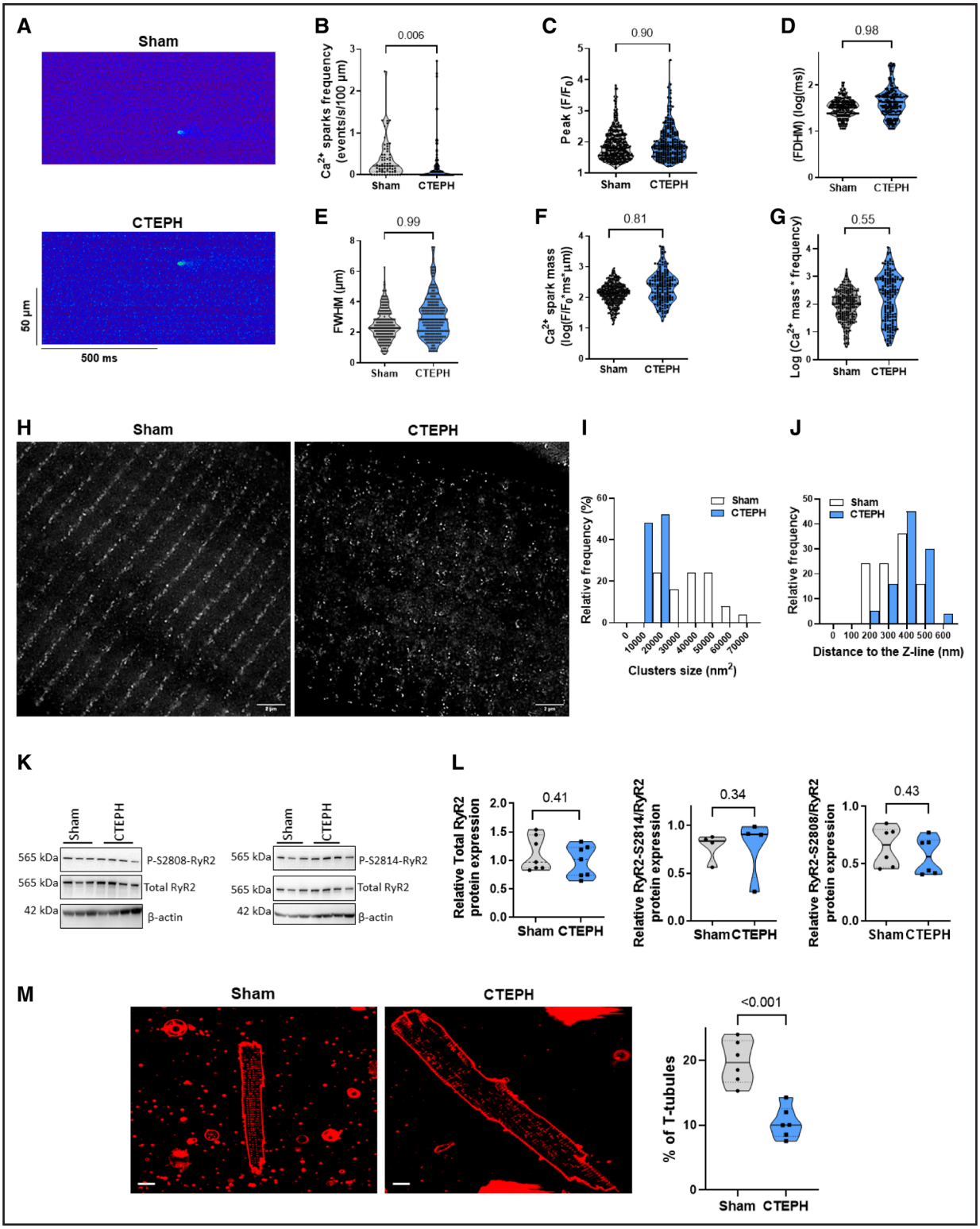

Figure 7. Intrinsic RyR2 (ryanodine receptor 2) cluster activity and structural organization in right ventricular (RV) cardiomyocytes from Sham and chronic thromboembolic pulmonary hypertension (CTEPH) pigs.

A, Representative line-scan images of Ca^{2+} sparks in quiescent RV cardiomyocytes loaded with Fluo-4/AM from Sham and CTEPH pigs. **B**, Average of Ca^{2+} spark frequency (number of sparks/s/100 µm) recorded in 65 cells from Sham and 119 cells from CTEPH pigs. Average of Ca^{2+} spark amplitude (peak F/F_0, **C**), full duration at half-maximum (FDHM, ms, **D**) and of full width at half-maximum (FWHM, µm, **E**) recorded in RV cardiomyocytes from Sham and CTEPH pigs (n=4–6 pigs, n=358–218 analyzed Ca^{2+} sparks). Average Ca^{2+} spark mass (F/F_0*ms*µm, **F**) and Ca^{2+} spark-mediated SR Ca^{2+} leak (Ca^{2+} spark mass*frequency, **G**) in RV cardiomyocytes from Sham and CTEPH pigs. **H**, Representative deconvoluted stimulated emission depletion images of RyR2 in RV cardiomyocytes from Sham and CTEPH pigs (Scale bar=2 µm). **I**, Clusters size relative frequency distribution in Sham or CTEPH cells. **J**, Clusters relative frequency distribution along the Z line in Sham or (*Continued*)

The Emergence of STIM1 Long Variant (STIM1L) Expression Is Associated With Enhanced SOCE in RV Cardiomyocytes From CTEPH Pigs

Recently, we and others reported that store-operated Ca^{2+} entry (SOCE) contributes to Ca^{2+} mishandling in LV and RV remodeling and dysfunction.[10,11] In LV failure (LVF), we showed that Orai1 inhibition is cardioprotective by preserving the SERCA2a expression and the SR Ca^{2+} load.[12] We thus investigated whether SOC molecules could be responsible for the Ca^{2+} cycling alteration in CTEPH pigs. As exemplified in Figure 8A, after SR Ca^{2+} depletion, the addition of extracellular Ca^{2+} induced a moderate SOCE in Sham cells. This SOCE was enhanced in CTEPH RV myocytes (Figure 8A). The classic form of STIM1 (stromal interaction molecule 1) protein and Orai1 protein was unchanged while the long form of STIM1, called STIM1L was re-expressed in all RV tissues from CTEPH pigs (Figure 8B), while no significant differences in STIM2, Orai2/3, TRPC1/C3/C4/C5, and TRPC6 protein expression were observed in RV tissue from Sham and CTEPH pigs (Figure S6). In addition, we found increased protein expression of STIM1 and STIM1L in RV tissue from patients with PAH, while no significant changes in Orai1 protein were observed (Figure 8C). We previously demonstrated that STIM1L/Orai1 function contributed to RV Ca^{2+} mishandling in rat PH models induced by monocrotaline exposure.[13] Based on this finding, we investigated whether the Orai1 function plays a role in Ca^{2+} cycling in the cardiomyocytes from CTEPH pigs. We found that selective Orai1 inhibition by JPIII (2 minutes of preincubation) did not significantly affect either the amplitude or decay time of $[Ca^{2+}]_i$ transients or cell shortening of pig RV cardiomyocytes in Sham condition (Figure S7A) and in CTEPH condition (Figure S7B).

DISCUSSION

In the present study, utilizing a pig model of RV dysfunction, we first determined a comprehensive transcriptomic signature of RV hypertrophy and dysfunction. We identified several molecular pathways associated with the extracellular matrix, energy metabolism, muscle contraction, hypertrophic markers, and other inflammatory factors with their key corresponding genes that are associated with the maladaptive phenotype of RV. We further validated the selected extracellular matrix molecules at the histological level with the increased fibrosis deposition, the deterioration of structural mitochondrial integrity by electron microscopy, and the RV dilation and dysfunction by echocardiography. We also showed several molecular pathways associated with the maladaptive phenotype of RV that are commonly dysregulated between the CTEPH pigs and patients with PAH with decompensated RV failure supporting the relevance of our model of RV dysfunction secondary to CTEPH in pigs.

Among these different dysregulated pathways, our unbiased transcriptome profiling revealed remodeling in Ca^{2+} actors and ion channels. We thus explored the Ca^{2+} homeostasis involved in excitation-contraction coupling and demonstrated evidence of Ca^{2+} homeostasis dysregulation in RV myocytes from CTEPH pigs.

Here, we showed that RV myocytes from CTEPH pigs have smaller I_{CaL} explained by the reduced expression of *CACNA1C* and auxiliary regulatory subunits. We also found that myocytes from CTEPH pigs have lower $[Ca^{2+}]_i$ transients associated with decreased SR Ca^{2+} content and cell shortening, as observed in many experimental LVF models.[12,14–16] The rate of rise of Ca^{2+} transients is also prolonged. This is probably associated with decreased I_{CaL} current density. Unlike in rodent cardiomyocytes, where Ca^{2+} release sites were homogeneous, we observed large areas of delayed Ca^{2+} release in CTEPH myocytes as in pig LV myocytes.[17] Indeed, CTEPH myocytes exhibit larger regions of delayed Ca^{2+} transients, both in number and size, compared with healthy RV myocytes. This dys-synchrony may be linked to a highly disorganized T-tubule network that we observed in CTEPH myocytes. This is in line with reduced density and disorganization of T-tubules found in LVF myocytes from myocardial infarction pigs, humans, and other experimental LVF animal models.[18–22]

In the RV context, we and others showed, in rat models, that the Ca^{2+} cycling modulation was also crucial in RV remodeling and dysfunction.[10,13] Most of these data were obtained from rodents with RV dysfunction due to progressive narrowing of pulmonary arteries. Only 1 study observed changes in Ca^{2+} signaling protein expression in the RV from humans with PAH,[23] suggesting an alteration in Ca^{2+} cycling.

In this CTEPH pig model, despite unaltered phospholamban abundance and phosphorylation levels, we found decreased SERCA2a protein expression. This could account for the lower SR Ca^{2+} content. Altered levels of SERCA2a have also been found in severe rodent models of RVF[24] and LVF.[12,25–27] In the end stage of RVF in

Figure 7 Continued. CTEPH cells. White bars indicate 24 797 clusters in 26 cells from 3 Sham pigs, and blue bars indicates 71 302 clusters in 56 cells from 2 CTEPH pigs. **K** and **L**, Representative Western blots and quantification of total RyR2, P-S2808-RyR2, and P-S2814-RyR2 normalized by the total RyR2 expression in RV tissues from Sham and CTEPH pigs (n=4–7 pigs). **M**, **Left**, Confocal images of the T-tubule network stained by Di-4ANEPPS in RV cardiomyocytes from Sham and CTEPH pigs (scale bar=10 µm). **Right**, Percentage of T-tubules under the cell surface in RV cardiomyocytes from Sham and CTEPH pigs (n=6 pigs). All the results are presented as violin plots showing all investigated cells or tissues with the minimum to maximum, with the median (line), and with first and third quartiles (dotted lines). Specific procedure analysis and output for each figure panel are given in Table S2, and no outliers were eliminated.

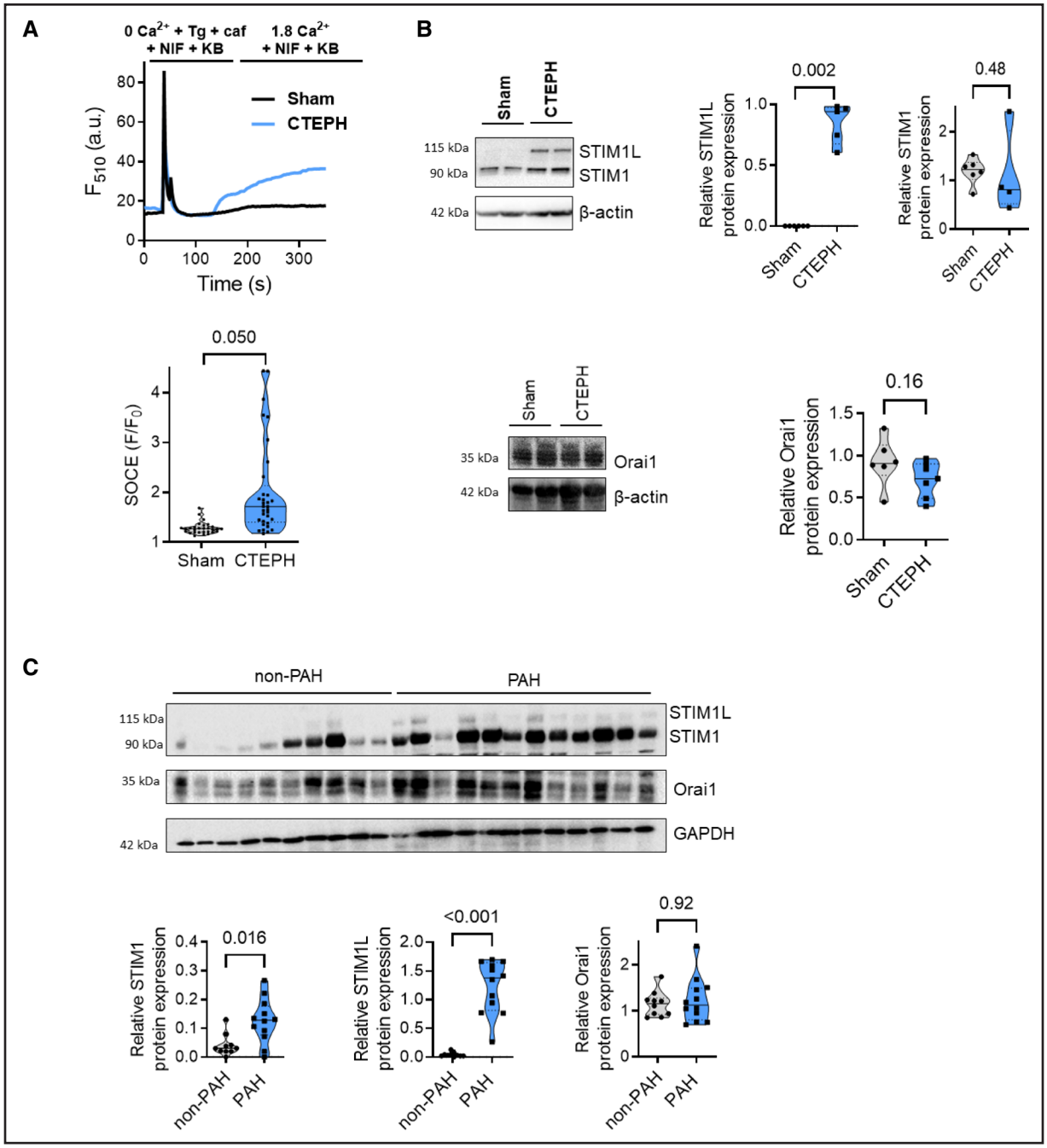

Figure 8. Store-operated Ca^{2+} entry (SOCE) machinery in right ventricular (RV) cardiomyocytes from Sham and chronic thromboembolic pulmonary hypertension (CTEPH) pigs.

A, **Top**, Representative traces of fluorescence variation in Fluo-4/AM-loaded RV cardiomyocytes. Cells were exposed to 5 µmol/L Tg+20 mmol/L caf in the presence of 10 µmol/L nifedipine (NIF) and 2 µmol/L KB-R7943 (KB) in Ca^{2+}-free medium, then to 1.8 mmol/L Ca^{2+}-containing solution to evaluate the SOCE in the presence of NIF and KB. **Bottom**, Quantitative assessment of SOCE amplitude (F/F_0) in RV cardiomyocytes from Sham and CTEPH pigs (n=3 pigs, n=29–32 investigated cells). **B**, Representative Western blot and quantification of STIM1L (stromal interaction molecule 1 long isoform), STIM1, and Orai1 protein expression in RV tissues from Sham and CTEPH pigs. β-Actin was used as the loading control (n=5–6 pigs). **C**, Representative Western blot and quantification of STIM1L, STIM1, and Orai1 protein expression in RV tissues from control and patients with pulmonary arterial hypertension (PAH). β-Actin was used as the loading control. n=10 patients with non-PAH and 12 patients with PAH. Specific procedure analysis and output for each figure panel are given in Table S2, and no outliers were eliminated.

human patients with PAH, SERCA2a and phospholamban phosphorylation (Thr17) protein expression were reduced compared with non-PAH patients.[23] Thus, the selective SERCA2a pharmacological approach should be considered for RVF, as previously proposed,[28,29] to counteract intracellular Ca^{2+} abnormalities.

The decrease in SR Ca^{2+} uptake, as proven by the decrease in SERCA2a expression, could also be explained by a progressive Ca^{2+} leak during the diastole. We found a decrease in the Ca^{2+} sparks frequency in CTEPH myocytes. This could be explained by the lower SR Ca^{2+} load or the low density of the T-tubules. Consequently, a significant number of RyR2 may not be coupled to the junctional SR. CaMKII-dependent phosphorylation at S2814 of RyR2 has been widely accepted to dysregulate RyR2 in a broad range of LVF models.[30,31] In our model, these modifications are not due to changes in RyR2 expression or phosphorylation at the PKA-mediated site or the CaMKII-mediated site.

As mentioned before, we reported a significant T-tubule loss in RV cardiomyocytes from CTEPH pigs. Moreover, by super-resolution stimulated emission-depletion super-resolution microscopy, we observed smaller RyR2 clusters and greater dispersion along the Z line, with a higher relative frequency of RyR2 clusters far from the line. Functionally, ultrastructural remodeling of the dyad leads to the formation of orphaned RyR2 clusters, and unrestricted Ca^{2+} sparks diffusion in the space, explaining the tendency to have wider and longer Ca^{2+} sparks in CTEPH myocytes. In postinfarction heart failure rats, the RyR2 clusters are also smaller, leading to the desynchronization of the overall Ca^{2+} transients.[32] Disturbances in RyR2 binding with junctophilin 2 have also been demonstrated to underlie ultrastructural remodeling of the dyad, leading to smaller RyR2 couplons in $RyR2^{R420Q}$ CPVT mutation.[33] The RyR2 nanostructure alteration thus could contribute to the Ca^{2+} transients and contraction alteration in the CTEPH model.

We previously demonstrated an upregulation of Orai1-mediated SOCE in a model of pressure overload that over-activates the Pyk2/MEK/ERK (proline-rich tyrosine kinase 2/mitogen-activated protein kinase/extracellular signal regulated kinase) pathway responsible for the reduced SERCA2a pump expression and LV systolic dysfunction, without affecting the hypertrophic process. Notably, we documented that functional Orai1 inhibition has a cardiac protective effect by preserving SR Ca^{2+} load and SERCA2a expression.[12] Moreover, STIM1L and Orai1 expression is enhanced in maladaptive RV cardiomyocytes from monocrotaline rats.[13] In this last study, in vitro pharmacological inhibition of Orai1 normalized Ca^{2+} handling and cardiomyocyte contractility to control levels.[13] Likewise, in vivo inhibition of Orai1 improved RV dysfunction in chronic hypoxia-, monocrotaline-, and Sugen/Hypoxia rat models.[34] Herein, whereas Orai1 expression is not altered in RV of CTEPH pig model and patients with PAH, we found enhanced SOCE associated with increased STIM1L expression in CTEPH myocytes. Selective Orai1 inhibition does not affect both Ca^{2+} transient amplitude and decay time or cell shortening in Sham and CTEPH conditions. This finding supports the idea that Orai1 has no role in Ca^{2+} cycling regulation in pigs in physiological conditions, as we previously reported in mice,[12] nor pathological conditions. This exacerbated SOCE may act on hypertrophic development, as previously proven in many LVF models.[10,35]

We conclude that the alteration in Ca^{2+} cycling, diastolic Ca^{2+} sparks, and SOCE machinery contribute to the RV remodeling and dysfunction in CTEPH pigs. These Ca^{2+} actors could constitute therapeutic targets to counteract the development of RV dysfunction.

LIMITATIONS

Access to isolated adult RV cardiomyocytes from patients with PAH or CTEPH is challenging, making functional assessments impossible. To our knowledge, we are not able to determine whether human RV failure leads to intracellular Ca^{2+} mishandling, as we found in our CTEPH pig model. The work done by Rain and colleagues suggested dysregulation of intracellular Ca^{2+} signaling (decreased SERCA2a and phospholamban phosphorylation (Thr17) protein expression).[23] However, they cannot confirm these results functionally. In our study, using the CTEPH pig models, we confirmed that the downregulation of SERCA2a expression is associated with reduced L-type Ca^{2+} channel expression and function, reduced Ca^{2+} transient amplitude, and reduced SR Ca^{2+} content contributing to RV loss of function in CTEPH pigs. We also found that SOCE machinery is dysregulated in RV cardiomyocytes from CTEPH pigs. Importantly, we confirmed that this alteration is also present in human RV tissues from patients with PAH. Some dysregulated genes are still unidentified using the transcriptomic database. Despite strong concordance between mRNA and protein abundance, we plan to conduct proteomic analysis because posttranslational regulations could explain some of the protein expression changes. Nevertheless, transcriptomic profiling is still a strong approach to quantify and understand the alterations of RV in experimental conditions. From a perspective, there would be an interest in deciphering the molecular and cellular processes involved in the transition from the adaptive to maladaptive stage. Finally, this study was conducted only on male pigs. PH affects more women than men, but the prognosis in men is worse. Thus, we also need to investigate the pathogenesis in female pigs submitted to chronic thromboembolism to suggest a potential sex-specific therapy.

ARTICLE INFORMATION

Received August 01, 2024; accepted March 24, 2025.

Affiliations

Université Paris-Saclay, Inserm, UMR-S 999, Hypertension Pulmonaire: Physiopathologie and Innovation Thérapeutique (HPPIT), AP-HP, Hôpital Bicêtre, Hôpital Marie Lannelongue (Groupe Hospitalier Paris Saint Joseph), ERN-LUNG, Le Plessis Robinson, France (F.A., B.M., G.F., G.R., A.S.-M.W., A.A., J. Grynblat, X.J., J.L.P., S.D.V., D.B., A.B., J. Guihaire, D.M., M.H., O.M.). Inserm, UMR-S 1180, Signalisation et Physiopathologie Cardiovasculaire, Université Paris-Saclay, Orsay,

France (R.L., R.P., F.L., G.G., A.-M.G., J.-P.B., J.S.). Service de Chirurgie Thoracique, Vasculaire et Transplantation Cardio-Pulmonaire, Hôpital Marie Lannelongue, Le Plessis Robinson, France (G.F., O.M.). Service de Chirurgie Cardiaque et Vasculaire, Hôpital Marie Lannelongue, Le Plessis Robinson, France (A.A., S.D.V., D.B., J. Guihaire). Service de Pneumologie et Soins Intensifs Respiratoires, Centre de Référence de l'Hypertension Pulmonaire, Le Kremlin-Bicêtre, France (X.J., D.M., M.H.). Service de Pneumologie et Transplantation Pulmonaire, Hôpital Marie Lannelongue, Le Plessis Robinson, France (J.L.P.). Université Paris-Saclay, Inserm, CNRS, Ingénierie et Plateformes au Service de l'Innovation Thérapeutique-Plateforme MIPSIT, Orsay, France (S.D.).

Acknowledgments

The authors thank Emy Ponsardin, Claudine Delomenie, and Florent Dumont for RNA sequencing experiments and bioinformatic analyses (ACTAGen and Bioinfo facilities, IPSIT Paris-Saclay University). The authors also acknowledge the sequencing and bioinformatics expertise of the I2BC High-throughput sequencing facility (Gif-sur-Yvette, France), supported by France Génomique (funded by the French National Program Investissement d'Avenir ANR-10-INBS-09). The authors thank Yvonne Dutheil from Inserm UMR-S999 and Hospital Marie Lannelongue for all her help. The authors thank France 2030 for the support. Drs Antigny, Grynblat, Mercier, and Sabourin participated in the research design. Drs Antigny, Luo, Perrier, Masson, Fadel, Ruffenach, Saint-Martin Willer, Akamkam, Grynblat, Jaïs, Brunet, Lefebvre, Gérard, Domenichini, Boët, Guihaire, and Sabourin conducted the experiments and performed the data analysis. All authors drafted the article for important intellectual content. All authors reviewed and revised the final version and approved the article submission.

Sources of Funding

This study was supported by grants from the French National Institute for Health and Medical Research (Inserm), the Université Paris-Saclay, the Marie Lannelongue Hospital, the Fédération Française de Cardiologie, the Fondation Maladies Rares AFM-Téléthon POCs(2023)-121503, and the French National Agency for Research (ANR; grants ANR-18-CE14-0023 [KAPAH], ANR-23-CE14-0009-02). Dr Humbert is supported by state funding managed by the National Research Agency according to the Investments for the Future program integrated into France 2030, under reference ANR-18-RHUS-0006 (DESTINATION 2024). Sham and CTEPH pigs were obtained with the financial support of RHU Destination 2024 (grant 18-RHUS-0006). Drs Masson and Saint-Martin Willer are supported by the Therapeutic Innovation Doctoral School (ED569). Dr Luo is supported by the Chinese Council Scholarship 2019.

Disclosures

Dr Humbert has relationships with drug companies, including Acceleron, AOP Orphan, Merck, Chiesi, Ferrer, Janssen, MorphogenIX, Shou Ti, Tiakis, and United Therapeutics. Dr Montani has relationships with drug companies, including Actelion, Bayer, GSK, Novartis, and Pfizer. Dr Jaïs has relationships with drug companies, including Janssen, Bayer, and Merck. In addition to being investigators in trials involving these companies, other relationships include consultancy services and memberships to scientific advisory boards. The other authors report no conflicts.

Supplemental Material

Tables S1–S7
Figures S1–S7
References 36–42

REFERENCES

1. Humbert M, Kovacs G, Hoeper MM, Badagliacca R, Berger RMF, Brida M, Carlsen J, Coats AJS, Escribano-Subias P, Ferrari P, et al; ESC/ERS Scientific Document Group. 2022 ESC/ERS Guidelines for the diagnosis and treatment of pulmonary hypertension. *Eur Respir J* 2023;61:2200879. doi: 10.1183/13993003.00879-2022
2. Vonk Noordegraaf A, Chin KM, Haddad F, Hassoun PM, Hemnes AR, Hopkins SR, Kawut SM, Langleben D, Lumens J, Naeije R. Pathophysiology of the right ventricle and of the pulmonary circulation in pulmonary hypertension: an update. *Eur Respir J*. 2019;53:1801900. doi: 10.1183/13993003.01900-2018
3. Andersen S, Nielsen-Kudsk JE, Vonk Noordegraaf A, de Man FS. Right ventricular fibrosis. *Circulation*. 2019;139:269–285. doi: 10.1161/CIRCULATIONAHA.118.035326
4. Llucià-Valldeperas A, de Man FS, Bogaard HJ. Adaptation and maladaptation of the right ventricle in pulmonary vascular diseases. *Clin Chest Med*. 2021;42:179–194. doi: 10.1016/j.ccm.2020.11.010
5. Humbert M, Lau EMT, Montani D, Jaïs X, Sitbon O, Simonneau G. Advances in therapeutic interventions for patients with pulmonary arterial hypertension. *Circulation*. 2014;130:2189–2208. doi: 10.1161/CIRCULATIONAHA.114.006974
6. Ponikowski P, Voors AA, Anker SD, Bueno H, Cleland JGF, Coats AJS, Falk V, González-Juanatey JR, Harjola VP, Jankowska EA, et al; ESC Scientific Document Group. 2016 ESC Guidelines for the diagnosis and treatment of acute and chronic heart failure: The Task Force for the diagnosis and treatment of acute and chronic heart failure of the European Society of Cardiology (ESC)Developed with the special contribution of the Heart Failure Association (HFA) of the ESC. *Eur Heart J*. 2016;37:2129–2200. doi: 10.1093/eurheartj/ehw128
7. Noly PE, Guihaire J, Coblence M, Dorfmüller P, Fadel E, Mercier O. Chronic thromboembolic pulmonary hypertension and assessment of right ventricular function in the piglet. *J Vis Exp*. 2015;105:e53133. doi: 10.3791/53133
8. Mercier O, Tivane A, Dorfmüller P, de Perrot M, Raoux F, Decante B, Eddahibi S, Dartevelle P, Fadel E. Piglet model of chronic pulmonary hypertension. *Pulm Circ*. 2013;3:908–915. doi: 10.1086/674757
9. Mercier O, Fadel E. Chronic thromboembolic pulmonary hypertension: animal models. *Eur Respir J*. 2013;41:1200–1206. doi: 10.1183/09031936.00101612
10. Sabourin J, Beauvais A, Luo R, Montani D, Benitah J-P, Masson B, Antigny F. The SOCE machinery: an unbalanced knowledge between left and right ventricular pathophysiology. *Cells*. 2022;11:3282. doi: 10.3390/cells11203282
11. Bartoli F, Sabourin J. Cardiac remodeling and disease: current understanding of STIM1/Orai1-mediated store-operated Ca2+ entry in cardiac function and pathology. *Adv Exp Med Biol*. 2017;993:523–534. doi: 10.1007/978-3-319-57732-6_26
12. Bartoli F, Bailey MA, Rode B, Mateo P, Antigny F, Bedouet K, Gerbaud P, Gosain R, Plante J, Norman K, et al. Orai1 channel inhibition preserves left ventricular systolic function and normal Ca2+ handling after pressure overload. *Circulation*. 2020;141:199–216. doi: 10.1161/CIRCULATIONAHA.118.038891
13. Sabourin J, Boet A, Rucker-Martin C, Lambert M, Gomez A-M, Benitah J-P, Perros F, Humbert M, Antigny F. Ca2+ handling remodeling and STIM1L/Orai1/TRPC1/TRPC4 upregulation in monocrotaline-induced right ventricular hypertrophy. *J Mol Cell Cardiol*. 2018;118:208–224. doi: 10.1016/j.yjmcc.2018.04.003
14. Val-Blasco A, Gil-Fernández M, Rueda A, Pereira L, Delgado C, Smani T, Ruiz Hurtado G, Fernández-Velasco M. Ca2+ mishandling in heart failure: Potential targets. *Acta Physiol (Oxf)*. 2021;232:e13691. doi: 10.1111/apha.13691
15. Song L-S, Sobie EA, McCulle S, Lederer WJ, Balke CW, Cheng H. Orphaned ryanodine receptors in the failing heart. *Proc Natl Acad Sci U S A*. 2006;103:4305–4310. doi: 10.1073/pnas.0509324103
16. Gómez AM, Valdivia HH, Cheng H, Lederer MR, Santana LF, Cannell MB, McCune SA, Altschuld RA, Lederer WJ. Defective excitation-contraction coupling in experimental cardiac hypertrophy and heart failure. *Science*. 1997;276:800–806. doi: 10.1126/science.276.5313.800
17. Heinzel FR, Bito V, Volders PGA, Antoons G, Mubagwa K, Sipido KR. Spatial and temporal inhomogeneities during Ca2+ release from the sarcoplasmic reticulum in pig ventricular myocytes. *Circ Res*. 2002;91:1023–1030. doi: 10.1161/01.res.0000045940.67060.dd
18. Yamakawa S, Wu D, Dasgupta M, Pedamallu H, Gupta B, Modi R, Mufti M, O'Callaghan C, Frisk M, Louch WE, et al. Role of t-tubule remodeling on mechanisms of abnormal calcium release during heart failure development in canine ventricle. *Am J Physiol Heart Circ Physiol*. 2021;320:H1658–H1669. doi: 10.1152/ajpheart.00946.2020
19. Lyon AR, MacLeod KT, Zhang Y, Garcia E, Kanda GK, Lab MJ, Korchev YE, Harding SE, Gorelik J. Loss of T-tubules and other changes to surface topography in ventricular myocytes from failing human and rat heart. *Proc Natl Acad Sci U S A*. 2009;106:6854–6859. doi: 10.1073/pnas.0809777106
20. Huang C, Chen B, Guo A, Chen R, Zhu Y, Kutschke W, Hong J, Song L. Sildenafil ameliorates left ventricular T-tubule remodeling in a pressure overload-induced murine heart failure model. *Acta Pharmacol Sin*. 2016;37:473–482. doi: 10.1038/aps.2016.13
21. Heinzel FR, Bito V, Biesmans L, Wu M, Detre E, von Wegner F, Claus P, Dymarkowski S, Maes F, Bogaert J, et al. Remodeling of T-tubules and reduced synchrony of Ca2+ release in myocytes from chronically ischemic myocardium. *Circ Res*. 2008;102:338–346. doi: 10.1161/CIRCRESAHA.107.160085
22. He J, Conklin MW, Foell JD, Wolff MR, Haworth RA, Coronado R, Kamp TJ. Reduction in density of transverse tubules and L-type Ca(2+) channels in canine tachycardia-induced heart failure. *Cardiovasc Res*. 2001;49:298–307. doi: 10.1016/s0008-6363(00)00256-x

23. Rain S, Bos D da SG, Handoko ML, Westerhof N, Stienen G, Ottenheijm C, Goebel M, Dorfmüller P, Guignabert C, Humbert M, et al. Protein changes contributing to right ventricular cardiomyocyte diastolic dysfunction in pulmonary arterial hypertension. *J Am Heart Assoc*. 2014;3:e000716.
24. Antigny F, Mercier O, Humbert M, Sabourin J. Excitation-contraction coupling and relaxation alteration in right ventricular remodelling caused by pulmonary arterial hypertension. *Arch Cardiovasc Dis*. 2020;113:70–84. doi: 10.1016/j.acvd.2019.10.009
25. Piper C, Bilger J, Henrichs EM, Schultheiss HP, Horstkotte D, Doerner A. Is myocardial Na+/Ca2+ exchanger transcription a marker for different stages of myocardial dysfunction? Quantitative polymerase chain reaction of the messenger RNA in endomyocardial biopsies of patients with heart failure. *J Am Coll Cardiol*. 2000;36:233–241. doi: 10.1016/s0735-1097(00)00703-8
26. Schwinger RH, Wang J, Frank K, Müller-Ehmsen J, Brixius K, McDonough AA, Erdmann E. Reduced sodium pump alpha1, alpha3, and beta1-isoform protein levels and Na+,K+-ATPase activity but unchanged Na+-Ca2+ exchanger protein levels in human heart failure. *Circulation*. 1999;99:2105–2112. doi: 10.1161/01.cir.99.16.2105
27. Val-Blasco A, Piedras MJGM, Ruiz-Hurtado G, Suarez N, Prieto P, Gonzalez-Ramos S, Gómez-Hurtado N, Delgado C, Pereira L, Benito G, et al. Role of NOD1 in Heart Failure Progression via Regulation of Ca2+ Handling. *J Am Coll Cardiol*. 2017;69:423–433. doi: 10.1016/j.jacc.2016.10.073
28. Arici M, Ferrandi M, Barassi P, Hsu S-C, Torre E, Luraghi A, Ronchi C, Chang G-J, Peri F, Ferrari P, et al. Istaroxime Metabolite PST3093 Selectively Stimulates SERCA2a and Reverses Disease-Induced Changes in Cardiac Function. *J Pharmacol Exp Ther*. 2023;384:231–244. doi: 10.1124/jpet.122.001335
29. Luraghi A, Ferrandi M, Barassi P, Arici M, Hsu S-C, Torre E, Ronchi C, Romerio A, Chang G-J, Ferrari P, et al. Highly selective SERCA2a activators: preclinical development of a congeneric group of first-in-class drug leads against heart failure. *J Med Chem*. 2022;65:7324–7333. doi: 10.1021/acs.jmedchem.2c00347
30. Houser SR. Role of RyR2 phosphorylation in heart failure and arrhythmias: protein kinase A-mediated hyperphosphorylation of the ryanodine receptor at serine 2808 does not alter cardiac contractility or cause heart failure and arrhythmias. *Circ Res*. 2014;114:1320–7; discussion 1327. doi: 10.1161/CIRCRESAHA.114.300569
31. Benitah J-P, Perrier R, Mercadier J-J, Pereira L, Gómez AM. RyR2 and calcium release in heart failure. *Front Physiol*. 2021;12:734210. doi: 10.3389/fphys.2021.734210
32. Kolstad TR, van den Brink J, MacQuaide N, Lunde PK, Frisk M, Aronsen JM, Norden ES, Cataliotti A, Sjaastad I, Sejersted OM, et al. Ryanodine receptor dispersion disrupts Ca2+ release in failing cardiac myocytes. *eLife*. 2018;7:e39427. doi: 10.7554/eLife.39427
33. Yin L, Zahradnikova A, Rizzetto R, Boncompagni S, Rabesahala de Meritens C, Zhang Y, Joanne P, Marqués-Sulé E, Aguilar-Sánchez Y, Fernández-Tenorio M, et al. Impaired binding to Junctophilin-2 and nanostructural alteration in CPVT mutation. *Circ Res*. 2021;129:e35–e52. doi: 10.1161/CIRCRESAHA.121.319094
34. Masson B, Le Ribeuz H, Sabourin J, Laubry L, Woodhouse E, Foster R, Ruchon Y, Dutheil M, Boët A, Ghigna M-R, et al. Orai1 inhibitors as potential treatments for pulmonary arterial hypertension. *Circ Res*. 2022;131:101161CIRCRESAHA122321041.
35. Luo R, Gomez AM, Benitah J-P, Sabourin J. Targeting orai1-mediated store-operated Ca2+ entry in heart failure. *Front Cell Dev Biol*. 2020;8:586109. doi: 10.3389/fcell.2020.586109
36. Mika D, Bobin P, Lindner M, Boet A, Hodzic A, Lefebvre F, Lechène P, Sadoune M, Samuel J-L, Algalarrondo V, et al. Synergic PDE3 and PDE4 control intracellular cAMP and cardiac excitation-contraction coupling in a porcine model. *J Mol Cell Cardiol*. 2019;133:57–66. doi: 10.1016/j.yjmcc.2019.05.025
37. Lambert M, Boet A, Rucker-Martin C, Mendes-Ferreira P, Capuano V, Hatem S, Adão R, Brás-Silva C, Hautefort A, Michel J-B, et al. Loss of KCNK3 is a hallmark of RV hypertrophy/dysfunction associated with pulmonary hypertension. *Cardiovasc Res*. 2018;114:880–893. doi: 10.1093/cvr/cvy016
38. Liao Y, Smyth GK, Shi W. The R package Rsubread is easier, faster, cheaper and better for alignment and quantification of RNA sequencing reads. *Nucleic Acids Res*. 2019;47:e47. doi: 10.1093/nar/gkz114
39. Chen Y, Lun ATL, Smyth GK. From reads to genes to pathways: differential expression analysis of RNA-Seq experiments using Rsubread and the edgeR quasi-likelihood pipeline. *F1000Res*. 2016;5:1438. doi: 10.12688/f1000research.8987.2
40. Ritchie ME, Phipson B, Wu D, Hu Y, Law CW, Shi W, Smyth GK. limma powers differential expression analyses for RNA-sequencing and microarray studies. *Nucleic Acids Res*. 2015;43:e47. doi: 10.1093/nar/gkv007
41. Dumont F, Ponsardin E, Bernadat G, Cohen-Kaminsky S. MOAL: Multi-Omic Analysis at Lab. A simplified methodology workflow to make reproducible omic bioanalysis. 2023. doi: 10.1101/2023.10.17.562686
42. Liberzon A, Birger C, Thorvaldsdóttir H, Ghandi M, Mesirov JP, Tamayo P. The Molecular Signatures Database (MSigDB) hallmark gene set collection. *Cell Syst*. 2015;1:417–425. doi: 10.1016/j.cels.2015.12.004